Power Synchronization of Smart Transformers Allowing Universal Operation in Radial and Meshed Grids

Zhixiang Zou, *Senior Member*, *IEEE*, Xingqi Liu, Jian Tang, Giovanni De Carne, *Senior Member*, *IEEE*, Marco Liserre, *Fellow*, *IEEE*, Zheng Wang, *Senior Member*, *IEEE*, and Ming Cheng, *Fellow*, *IEEE*

***Abstract*—The Smart Transformer (ST) is a solid-state transformer with control and communication functionalities, interfacing medium voltage and low voltage grids. The ST can independently operate in a radial network configuration, and also in a meshed grid operation. The meshed operation has high potential to optimize the power flow in the network, avoiding or postponing the reinforcement of distribution grids. Nevertheless, the control and synchronization during the meshed operation are not trivial. The perturbation of the voltage in transition between the two operations is inevitable. This could lead to uncontrolled power flow and endanger the meshed operation. Moreover, the stability of the meshed grid has seldom been studied. To address these issues, this paper proposes a voltage control with power-based synchronization for the ST. This allows the universal operation of both radial and meshed grids, while ensuring smooth transition. Modeling and stability analysis of such a system are investigated to make sure of safe operation. Simulation and experimental results are provided to validate the effectiveness of the proposed control and theoretical analysis.**

***Index Terms*—Meshed operation, smart transformer, solid-state transformer, stability, synchronization, voltage control.**

I. Introduction

THE Smart Transformer (ST) is essentially a power-electronics-based solid-state transformer, being adopted as an intelligent substation with control and communication functionalities, which interfaces medium voltage (MV) grid and low voltage (LV) one [1]. Compared to the conventional distribution grid, the ST-fed grid offers connection to hybrid grid and is able to improve the demand-response balance. Besides, various ancillary services can be provided to MV/LV grids, which make it possible to increase the reliability and hosting capacity of the electric grid [2]. More importantly, the ST can mesh the LV grids, being ringed at the LVAC buses or at the terminal of the LV ac feeders. This offers high potential to optimize the power flow in the network, avoiding or postponing the reinforcements of distribution grids. As reported in the "LV-ENGINE" project funded by Scottish Power [3], it is estimated that the ST can save up to £60 M in grid upgrade costs by 2030, and avoid construction of 16 % new substations.

To achieve meshed operation, the control and synchronization of ST is not trivial [4]. The ST-fed grid and the feeder to be meshed are usually not synchronized in terms of different voltage amplitudes, frequencies, and phase sequencing. This could lead to an uncontrolled power flow in the network after closing the switch between the two feeders [5]. Similar problems can be found in the reconnection of microgrid to the utility, from the islanding mode to the grid-connected mode. It is expected that the microgrid can transit seamlessly between these two modes. Several approaches have been proposed to achieve the smooth operation during transition. One of the most common ways is to control the power converter as a grid-forming converter during islanding mode, and then switch it to be a grid-following converter when connecting to the grid [6]–[9]. In the application of ST, some similar works have been done by using two sets of control strategies in different scenarios to guarantee seamless transition between radial and meshed operation [10], [11]. However, these approaches requires a complex control structure and parameter tuning is not trivial to guarantee high performance and stability before and after the mode transition.

On the other hand, in recent literature, a power converter can behave as a grid-forming converter before and after the reconnection of the microgrid [12]–[14]. With respect to the grid-forming converter, several control strategies including droop control [12], [13], self-synchronized synchronverter [14], can be employed. Most of these control strategies do not require a PLL-based synchronization, but power-based synchronization instead [15]. Comparing to the scheme switch between grid-forming and grid-following converter, the complex control structure and parameter tuning can be saved by using this type of approach, and thus the perturbations associated with the control transition can be largely reduced. Nevertheless, the perturbation of the voltage in terms of phase angle is

Manuscript received March 29, 2021; revised May 23, 2021; accepted August 2, 2021. Date of online publication May 6, 2022; date of current version April 15, 2022. This work was supported by the National Natural Science Foundation of China under Grant 52377171.

Z. X. Zou (corresponding author, email: zzou@seu.edu.cn; ORCID: https://orcid.org/0000-0002-3837-3334), X. Q. Liu, J. Tang, Z. Wang, and M. Cheng are with the School of Electrical Engineering, Southeast University, Nanjing 210096, China.

G. De Carne is with the Institute for Technical Physics, Karlsruhe Institute of Technology, Karlsruhe, Germany.

M. Liserre is with the Chair of Power Electronics, Kiel University, Kiel, Germany.

DOI: 10.17775/CSEEJPES.2021.02350

still inevitable, which could endanger the meshed operation of the distribution grid. Moreover, the power setpoints of a grid-forming converter before and after reconnection must be dedicatedly given to ensure 1) the expected power flow and 2) synchronization during transition. The design criterion of the power setpoints with these considerations is still missing.

To address these issues, this paper proposes a voltage control strategy using power-based synchronization for the ST-fed grid, allowing universal operation in both radial and meshed grids. In particular, the synchronization mechanism before and after the NOP closure is presented, which facilitates seamless transition. The design of power setpoints of the ST LV converter in different scenarios is given to ensure grid-forming capability, and power flow regulation. Moreover, the modeling of the ST LV converter as well as the meshed grid is developed, and the system stability is studied, especially when converter-interfaced devices are being connected to the grid.

The paper structure is organized as follows. The system configuration of an ST-fed grid for radial and meshed operation is given in Section II. Then, the control and synchronization mechanism of the ST LV converter for the universal operation are proposed in Section III. Modeling and stability analysis of the grid as well as the connected grid converters are presented in Section IV. Simulation and experimental results are provided in Section V to validate the effectiveness of the proposed control scheme. Conclusions are drawn in Section VI.

II. System Configuration

The system configuration of a two-feeder radial distribution grid is presented in Fig. 1, where the two feeders are fed by an ST and a conventional power transformer (CPT), respectively. Different types of devices including loads, electric vehicles (EVs) and distributed energy resources (DERs) are connected to the feeders. Two normally open point (NOP) switches are utilized to connect the two feeders, one at the LVAC buses and the other at the terminal of the feeders. During normal operation, the NOP switches are open so that each feeder is fed by its own transformer. Under some circumstances, for instance, current congestion or maintenance, one of the switches can be closed to achieve meshed operation. This facilitates the power flow regulation between the two substations, so that the voltage profile and current flow can be better managed.

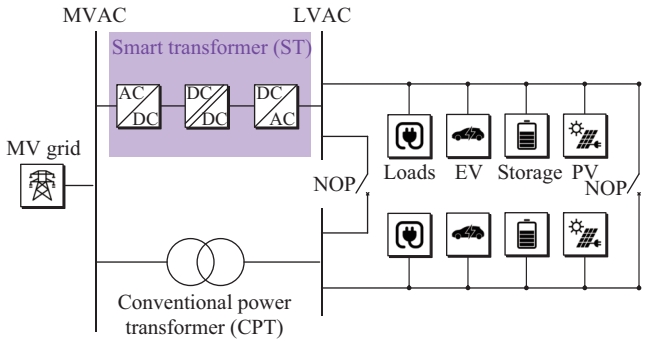

Fig. 1. Two-feeder radial distribution grid fed by ST and CPT.

The whole procedure of the closure of NOP switch is illustrated in Fig. 2. The control and synchronization requirements

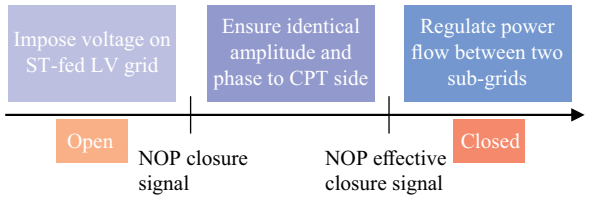

Fig. 2. Control and synchronization requirements of ST LV converter with different NOP conditions.

at each stage are given in the figure as well. Initially, the ST, or more specifically, the ST LV converter imposes three-phase sinusoidal voltage waveforms on its LV grid, and the CPT feeds the connected feeder(s) independently. In case of CPT being overloaded (i.e., CPT current exceeds the security limit), an NOP closure signal will be sent to the ST. As soon as the ST receives the signal, it has to not only impose voltage as usual but also synchronize its voltage amplitude and phase angle with the CPT side. At this stage, the amplitude and phase of ST voltage should be modified in a smooth way complying with the grid codes, to ensure normal operation of the connected devices. When the amplitudes and phases of the two feeders are identical, the NOP switch can be effectively closed without any problem.

After the effective closure of NOP switch, the power flow between the two feeders can be regulated. At this stage, the ST LV converter has to impose voltage to the connected devices while optimizing the power flow of the distribution grid. In the scenario of overloading CPT, the ST can increase the power transmission from the MV grid to the LV one, reacting to the CPT current. The increasing of power transmission allows the ST to alleviate the CPT overload issue by transferring power from ST side to the CPT feeder. Eventually, the power flow of the overall distribution grid reaches a new equilibrium and an overload of the CPT can be avoided. It is worth noting that the power flow through the NOP switch is bidirectional. This indicates the ST overload can be avoided as well by absorbing power from the CPT side through the NOP switch.

III. Proposed Control Strategy for Universal Operation

To achieve the control and synchronization targets, the control strategy of ST LV converter is proposed in this section. For the sake of simplicity, the impact of the MV converter as well as dc/dc converter have been neglected thanks to the decoupling effect of dc-links. A simplified model of the CPT is used, where an equivalent voltage source is in series with inductor.

The detailed control strategy is presented in Fig. 3, where ΔP and ΔQ indicate the active and reactive power exchanges between the two sub-grids (or two feeders). Since the power exchange through the NOP switch is bidirectional, ΔP and ΔQ can be both positive and negative. To synchronize with the CPT side, the power-based synchronization (power sync.) and its auxiliary controller (highlighted in blue in Fig. 3) are proposed. After the effective closure of NOP switch, the power setpoints block and the power-based synchronization are responsible for power flow regulation. The output of

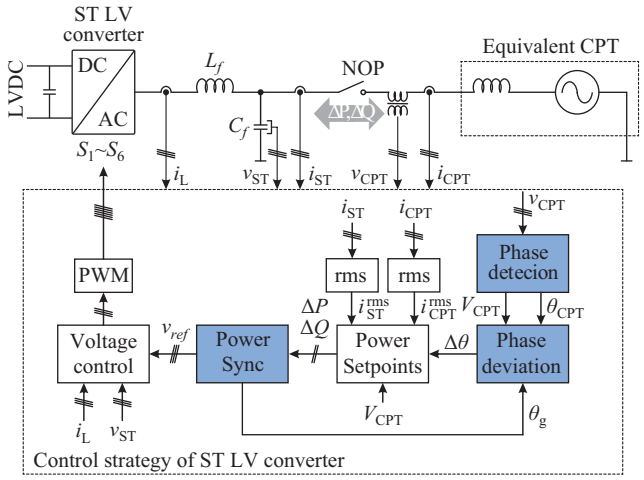

Fig. 3. Proposed control scheme of ST LV converter.

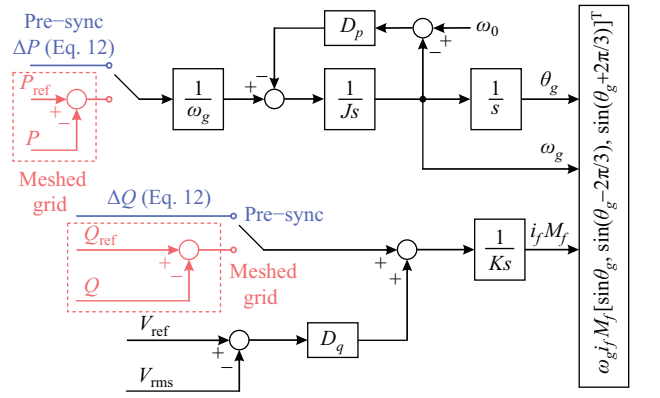

Fig. 4. Power-based synchronization of ST LV converter using virtual synchronous machine concept.

the power-based synchronization is the three-phase reference voltage for the ST LV converter, which is regulated by the voltage control during the whole process.

A. Power-based Synchronization

The functionalities of the power-based synchronization include: 1) allowing the ST LV converter to presynchronize with the CPT voltage before the switch is closed; 2) synchronization and facilitating power flow regulation after the switch is closed. In this regard, the power-based synchronization design is derived from the virtual synchronous machine concept [15]. The back electromotive force (EMF) refers to the average value of the terminal voltage of the LV converter, which is

$$e_{\mathrm{abc}} = M_f i_f \omega_{\mathrm{g}} \widetilde{\sin}\theta_{\mathrm{g}} \tag{1}$$

where M_f is the mutual inductance, i_f is the rotor excitation current, ω_{g} is the rotor speed, θ_{g} is the rotor angle, and $\widetilde{\sin}\theta_{\mathrm{g}} = [\sin\theta_{\mathrm{g}}, \sin(\theta_{\mathrm{g}} - 2\pi/3), \sin(\theta_{\mathrm{g}} + 2\pi/3)]^T$.

The swing equation can be defined by

$$\frac{d\omega_{\mathrm{g}}}{\mathrm{d}t} = \frac{1}{J}(T_m - T_e - D_p\omega_{\mathrm{g}}) \tag{2}$$

where J is the moment of inertia, T_m is the mechanical torque, T_e is the electromagnetic torque, and D_p is a damping factor. For the LV converter, T_m can be regarded as the control input, and T_e can be given by

$$T_e = M_f i_f \langle i_{\mathrm{abc}}, \widetilde{\sin}\theta_{\mathrm{g}} \rangle \tag{3}$$

where i_{abc} is the three-phase converter current, $\langle\cdot,\cdot\rangle$ denotes the conventional inner product in $\mathbb{R}^3$. By combining (1)–(3), the power-based synchronization of the ST LV converter using the virtual synchronous machine concept can be developed and presented in Fig. 4.

One of the main control objectives of the ST LV converter is to regulate the power flow between the two feeders. The power flow can eventually refer to the power increment or decrement of the ST LV converter. For this reason, the difference ΔT between the control input (e.g., T_m) and its measurement (e.g., T_e) can be directly used as the input of the active power loop, which is obtained by

$$\Delta T = T_m - T_e = \frac{1}{\omega_{\mathrm{g}}}(P_{\mathrm{ref}} - P) = \frac{1}{\omega_{\mathrm{g}}}\Delta P \tag{4}$$

On the other hand, in order to obtain $M_f i_f$, the control loop of reactive power is designed, as shown in Fig. 4. Likewise active power loop, the increment or decrement of reactive power ΔQ is used as the control input, which indicates the reactive power flow between the two feeders. Moreover, to guarantee the grid-forming capability, the error between the voltage reference and the actual voltage amplitude is regulated by means of the reactive power loop. The error is multiplied with a voltage-drooping coefficient D_{q} and added to the reactive power loop, which is described by

$$M_f i_f = \frac{1}{Ks}[\Delta Q + D_{\mathrm{q}}(V_{\mathrm{ref}} - V_{\mathrm{amp}})] \tag{5}$$

where V_{ref} is the nominal amplitude of voltage, and V_{amp} is the actual amplitude, which can be measured by various amplitude detectors, and K is the K factor for the reactive power loop.

B. Phase Detection and Deviation

Before the switch is closed, a presynchronized procedure is required to align the ST voltage (specifically its phase angle) with the CPT voltage. To achieve the target, the phase detection and deviation blocks are employed to obtain the amplitude and phase angle of the CPT secondary voltage and to calculate the phase/amplitude deviation between the ST and the CPT voltage. A synchronous reference frame phase-locked loop (SRF-PLL) is adopted as the phase detection block. Ignoring the sampling delay, both the amplitude v_{CPTd} and phase angle θ_{CPT} of the CPT secondary voltage can be measured online by means of the SRF-PLL, and then compared with those of the ST voltage during the presynchronized procedure.

When the ST starts to presynchronize with the CPT side, v_{CPTd} can be used as the voltage reference amplitude of the ST LV converter. Meanwhile, the phase deviation between θ_{g} (of ST) and θ_{CPT} (of CPT) has to be calculated by using the proposed phase deviation block. The phase deviation can be further utilized to calculate the active power setpoint of the

ST during this stage. The phase angles are usually triangular waveforms and phase deviation can not be calculated by subtraction. To address this issue, a multiplication of trigonometric functions of the two phase angles is first calculated as follows:

$$\sin\theta_{\rm g}\cos\theta_{\rm CPT} = \frac{1}{2}[\sin(\theta_{\rm g}+\theta_{\rm CPT}) + \sin(\theta_{\rm g}-\theta_{\rm CPT})] \quad (6)$$

Assuming phase deviation between the two feeders is small enough, one can get $\sin(\theta_{\rm g}-\theta_{\rm CPT}) \approx \theta_{\rm g}-\theta_{\rm CPT}$, and (6) can be rewritten by

$$\begin{aligned}\sin\theta_{\rm g}\cos\theta_{\rm CPT} &\approx \frac{1}{2}[\sin(\theta_{\rm g}+\theta_{\rm CPT}) + \theta_{\rm g}-\theta_{\rm CPT}] \\ &= \frac{1}{2}\sin(\theta_{\rm g}+\theta_{\rm CPT}) + \frac{\Delta\theta}{2} \end{aligned} \quad (7)$$

where $\Delta\theta$ is the phase deviation between the two sub-grids.

The result of the multiplication includes two terms: dc component $\Delta\theta/2$ and a twice fundamental frequency sinusoidal component $\frac{1}{2}\sin(\theta_{\rm g}+\theta_{\rm CPT})$. To remove the sinusoidal component, a low-pass filter can be used and the output is pure dc component $\Delta\theta/2$, which is proportional to the actual phase deviation.

C. Design of Power Setpoints

During the normal operation, the NOP switch is open. The power flow between the two feeders do not exist and is not required, and thus the setpoints for the active and reactive power loops (ΔP, ΔQ) are both zero. Under this circumstance, the ST voltage is controlled with fixed frequency ω_0 and amplitude $V_{\rm ref}$. The power flow from the MV grid to the LV one is adaptive to the load condition of the ST-fed grid.

When the ST receives the NOP closure signal, the presynchronized procedure begins. Since the switch is open, the power flow between the two feeders physically does not exist. Nevertheless, in order to adjust the phase angle and amplitude of the ST smoothly, virtual power flow (i.e., power setpoints) are required. Assuming the line impedance is inductive, active and reactive power setpoints are proportional to phase deviation and voltage amplitude, respectively, and can be described by

$$\begin{aligned}\Delta P &= \frac{V_{ST}V_{\rm CPT}}{X_{\rm eq}}\sin\Delta\theta \approx \frac{V_{ST}V_{\rm CPT}}{X_{\rm eq}}\Delta\theta = K_p\Delta\theta \\ \Delta Q &= \frac{V_{ST}V_{\rm CPT}\cos\Delta\theta - V_{\rm CPT}^2}{X_{\rm eq}} = K_{\rm q}V_{\rm CPT}\end{aligned} \quad (8)$$

where $X_{\rm eq}$ is the equivalent line impedance, K_p and $K_{\rm q}$ are the proportional gains of the active and reactive power setpoints.

According to (8), the active and reactive power setpoints during the presynchronized procedure are calculated by multiplying $\Delta\theta$ and $V_{\rm CPT}$ with K_p and $K_{\rm q}$. It is worth noting that the power setpoints at this stage are used for synchronization but not for power control. They do not refer to physical power exchange through the switch and will not affect the actual power flow in the distribution grid. In this regard, the gains of K_p and $K_{\rm q}$ do not have to be rigorously calculated based on (8) in practice. In general, higher K_p and $K_{\rm q}$ lead to faster convergence rate of phase and amplitude deviations between the two feeders, while on the other hand could incur instability. Therefore, a trade-off between convergence rate and stability has to be made for optimal K_p and $K_{\rm q}$.

When phase and amplitude deviations become zero, the NOP switch can be effectively closed. As soon as the switch is closed, the power flow between the two feeders can be regulated by means of the ST LV converter. At this stage, as shown in Fig. 4, the measured active and reactive power (P and Q) of the ST side are regulated by the active and reactive power loops, following the setpoints $P_{\rm ref}$ and $Q_{\rm ref}$. Different active power setpoint curves can be employed depending on different scenarios and grid codes. In this paper, the scenario of overload CPT and power setpoints will be discussed. In case of CPT overloading, while the ST is under partial load condition, power can be delivered from the ST LV bus to the CPT side so CPT overloading can be mitigated, and vice versa.

IV. Stability Analysis of Meshed Operation

Devices with PLL-synchronized converters are widely used in distribution grids [16], for instance, DERs, EV chagrining stations. It has been confirmed in literature that the PLL-synchronized converters suffer from stability issues particularly in weak grid conditions [17], [18]. For this reason, the interaction between the PLL-synchronized converter and the ST LV converter, as well as the CPT, will be analyzed in this section.

The impacts of the control loops of a PLL-synchronized converter on an ST LV converter (or grid-forming converter) have been already studied in literature [19], [20]. Instead, this paper focuses on the influence of the PLL-based synchronization on the ST LV converter and therefore, a simplified representation of a PLL-synchronized converter is given in Fig. 5(a). The PLL-synchronized converter is simplified as a controlled current source, whose current is calculated by transforming the current reference $\boldsymbol{I}_{\rm ref}$ from the dq to the abc frame. On the other hand, the ST LV converter is assumed to behave as a controlled voltage source, whose voltage is regulated by the proposed voltage control strategy presented in Section III. $\boldsymbol{Z}_{\rm l1}$/$\boldsymbol{Z}_{\rm l2}$ and $\boldsymbol{Z}_{\rm lo}$ represent line impedance and load impedance of the grid.

Based on the system representation, equivalent impedance-based model of the system is shown in Fig. 5(b), where $\boldsymbol{I}_{\rm eq}$ and $\boldsymbol{Y}_{\rm eq}$ are the equivalent current source and admittance of the PLL-synchronized converter, $\boldsymbol{V}_{\rm eq}$ and $\boldsymbol{Z}_{\rm eq}$ are the equivalent voltage source and impedance of the ST LV converter. The impedance-based modeling of both PLL-synchronized converter and ST LV converter are given as follows.

A. System Modeling

The equivalent impedance-based model of a PLL-synchronized converter is highlighted in blue in Fig. 5(b). Using the linearization of PLL reported in [18], the model in dq frame can be represented by

$$\boldsymbol{Y}_{\rm eq}(s) = \begin{bmatrix} 0 & I_{\rm q}G_{\rm PLL}(s) \\ 0 & -I_{\rm d}G_{\rm PLL}(s) \end{bmatrix} \quad (9)$$

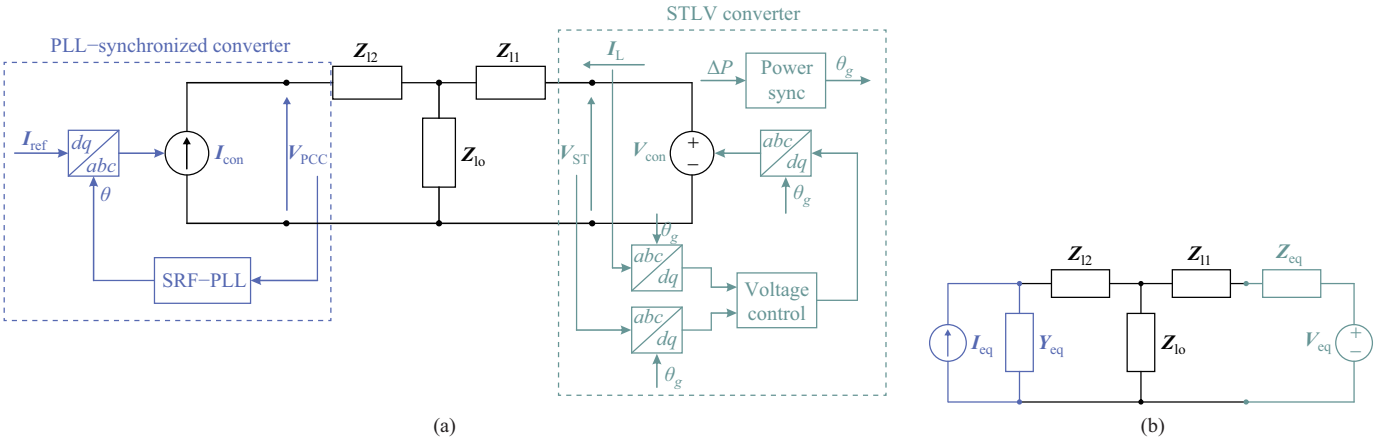

Fig. 5. System under study: (a) simplified representation including control and synchronization and (b) equivalent impedance-based model.

where I_{d} and I_{q} are the dc quantities of the converter current in the dq frame, and G_{PLL} is the q-axis transfer function of SRF-PLL, which is

$$G_{\mathrm{PLL}} = \frac{\Theta(s)}{V_{\mathrm{q}}(s)} = \frac{H_{\mathrm{PLL}}(s)}{1 + V_{\mathrm{d}} \cdot H_{\mathrm{PLL}}(s)} \tag{10}$$

Here, V_{d} is the dc quantity of the d-axis PCC voltage, and $H_{\mathrm{PLL}}(s) = H_{\mathrm{PI}}(s)/s$, H_{PI} is the transfer function of PI controller of SRF-PLL.

Then, the equivalent impedance-based model of the ST LV converter highlighted in green in Fig. 5(b) will be derived. According to the power-based synchronization and the voltage control, one can easily get

$$\begin{aligned}\begin{bmatrix}\Delta v_{\mathrm{d}}\\ \Delta v_{\mathrm{q}}\end{bmatrix} &= \boldsymbol{V}_{\mathrm{eqc}}\begin{bmatrix}\Delta v_{\mathrm{refd}}\\ \Delta v_{\mathrm{refq}}\end{bmatrix} + \boldsymbol{Z}_{\mathrm{eqc}}\begin{bmatrix}\Delta i_{\mathrm{d}}\\ \Delta i_{\mathrm{q}}\end{bmatrix} + \boldsymbol{\Theta}_{\mathbf{eq}}\Delta\theta_{\mathrm{g}}\\ &= \begin{bmatrix}V_{\mathrm{dd}}^{\mathrm{eqc}} & 0\\ 0 & V_{\mathrm{qq}}^{\mathrm{eqc}}\end{bmatrix}\begin{bmatrix}\Delta v_{\mathrm{refd}}\\ \Delta v_{\mathrm{refq}}\end{bmatrix} + \begin{bmatrix}Z_{\mathrm{dd}}^{\mathrm{eqc}} & Z_{\mathrm{dq}}^{\mathrm{eqc}}\\ Z_{qd}^{\mathrm{eqc}} & Z_{\mathrm{qq}}^{\mathrm{eqc}}\end{bmatrix}\begin{bmatrix}\Delta i_{\mathrm{d}}\\ \Delta i_{\mathrm{q}}\end{bmatrix}\\ &\quad + \begin{bmatrix}\Theta_{\mathrm{eqd}}\\ \Theta_{\mathrm{eqq}}\end{bmatrix}\Delta\theta_{\mathrm{g}}\end{aligned} \tag{11}$$

where $\boldsymbol{V}_{\mathrm{eqc}}$ represents the nature of the voltage control, which is essentially the closed-loop transfer function matrix of the voltage control of ST LV converter; $\boldsymbol{Z}_{\mathrm{eqc}}$ is the equivalent impedance when only considering the effect of voltage control; $\boldsymbol{\Theta}_{\mathbf{eq}}$ has the feature of power-based synchronization.

According to Fig. 4, the transfer function from ΔP to $\Delta\theta_{\mathrm{g}}$ can be derived as follows:

$$G_{\mathrm{vsg}}(s) = \frac{\Delta\theta_{\mathrm{g}}}{\Delta P} = \frac{1}{\omega_{\mathrm{g}} s(Js + D_p)} \tag{12}$$

The small-signal equation of active power calculation can be obtained by

$$\Delta P = \begin{bmatrix}I_{\mathrm{d}} & I_{\mathrm{q}}\end{bmatrix}\begin{bmatrix}\Delta v_{\mathrm{d}}\\ \Delta v_{\mathrm{q}}\end{bmatrix} + \begin{bmatrix}V_{\mathrm{d}} & V_{\mathrm{q}}\end{bmatrix}\begin{bmatrix}\Delta i_{\mathrm{d}}\\ \Delta i_{\mathrm{q}}\end{bmatrix} \tag{13}$$

and $\Delta\theta_{\mathrm{g}}$ can be rewritten by

$$\Delta\theta_{\mathrm{g}} = G_{\mathrm{vsg}}\begin{bmatrix}I_{\mathrm{d}} & I_{\mathrm{q}}\end{bmatrix}\begin{bmatrix}\Delta v_{\mathrm{d}}\\ \Delta v_{\mathrm{q}}\end{bmatrix} + G_{\mathrm{vsg}}\begin{bmatrix}V_{\mathrm{d}} & V_{\mathrm{q}}\end{bmatrix}\begin{bmatrix}\Delta i_{\mathrm{d}}\\ \Delta i_{\mathrm{q}}\end{bmatrix} \tag{14}$$

Substituting (14) into (11), the full model of ST LV converter is obtained:

$$\begin{aligned}\begin{bmatrix}\Delta v_{\mathrm{d}}\\ \Delta v_{\mathrm{q}}\end{bmatrix} &= \boldsymbol{V}_{\mathrm{eq}}\begin{bmatrix}\Delta v_{\mathrm{refd}}\\ \Delta v_{\mathrm{refq}}\end{bmatrix} + \boldsymbol{Z}_{\mathrm{eq}}\begin{bmatrix}\Delta i_{\mathrm{d}}\\ \Delta i_{\mathrm{q}}\end{bmatrix}\\ &= \begin{bmatrix}V_{\mathrm{dd}} & V_{\mathrm{dq}}\\ V_{qd} & V_{\mathrm{qq}}\end{bmatrix}\begin{bmatrix}\Delta v_{\mathrm{refd}}\\ \Delta v_{\mathrm{refq}}\end{bmatrix} + \begin{bmatrix}Z_{\mathrm{dd}} & Z_{\mathrm{dq}}\\ Z_{qd} & Z_{\mathrm{qq}}\end{bmatrix}\begin{bmatrix}\Delta i_{\mathrm{d}}\\ \Delta i_{\mathrm{q}}\end{bmatrix}\end{aligned} \tag{15}$$

where $\boldsymbol{V}_{\mathrm{eq}}$ and $\boldsymbol{Z}_{\mathrm{eq}}$ are the equivalent voltage source and impedance including the effect of power-based synchronization.

It can be seen that $\Delta\theta_{\mathrm{g}}$-related terms of (11) contribute to the equivalent impedance $\boldsymbol{Z}_{\mathrm{eq}}$. This indicates features of equivalent impedance can be changed when considering the effect of power-based synchronization. Comparisons of Bode plots of $\boldsymbol{Z}_{\mathrm{eqc}}$ (without the effect of synchronization) and $\boldsymbol{Z}_{\mathrm{eq}}$ (with the effect of synchronization) are carried out. It is observed that both the magnitude and the phase of Z_{qd} in the low-frequency range have been significantly modified when the effect of power-based synchronization is included, and they can be further altered by varying the damping factor D_p, shown in Fig. 6. In this regard, the effect of power-based synchronization has to be considered in the stability evaluation.

B. Stability Evaluation

The impedance ratio between the grid impedance and impedance of PLL-synchronized converter is

$$\boldsymbol{L} = \boldsymbol{Z}_{\mathrm{g}} \cdot \boldsymbol{Y}_{\mathrm{eq}} \tag{16}$$

where $\boldsymbol{Z}_{\mathrm{g}}$ is the equivalent grid impedance seen from the PCC of PLL-synchronized converter. According to the impedance-based model of Fig. 5(b), it can be calculated by

$$\boldsymbol{Z}_{\mathrm{g}} = \boldsymbol{Z}_{\mathrm{l2}} + (\boldsymbol{Z}_{\mathrm{eq}} + \boldsymbol{Z}_{\mathrm{l1}}) // \boldsymbol{Z}_{\mathrm{lo}} \tag{17}$$

in the case of ST-fed grid, while in a CPT-fed grid the $\boldsymbol{Z}_{\mathrm{eq}}$ can be formed by the equivalent inductance (L_T) and resistance (r_T) of CPT.

Using (15) and applying generalized Nyquist criterion to (16), one can obtain the system characteristic loci of an ST-fed grid with PLL-synchronized converter. None of them encircles

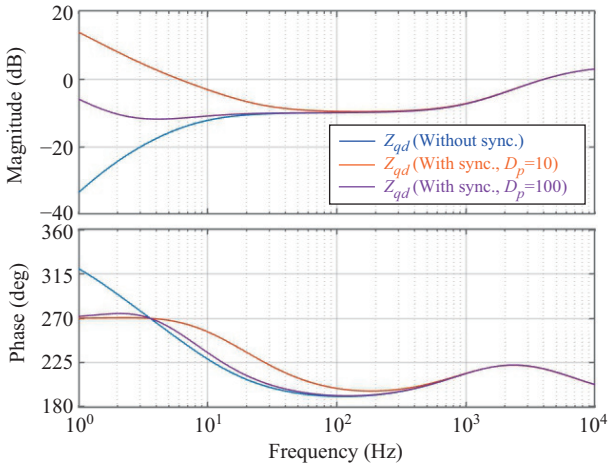

Fig. 6. Comparisons of equivalent *qd*-axis impedance (Z_{qd}) of ST LV converter in the *dq* frame with/without consideration of power-based synchronization.

the critical point $(-1,\ j0)$, indicating the system is stable. When using the CPT, the system characteristic loci of a CPT-fed grid with PLL-synchronized converter can be obtained and one of them (λ_2) encircles the critical point, which indicates the system is unstable. The comparisons of λ_2 of both case studies are presented in Fig. 7. It is shown that the ST-fed grid can offer a stronger network for the PLL-synchronized converter with the concern of stability.

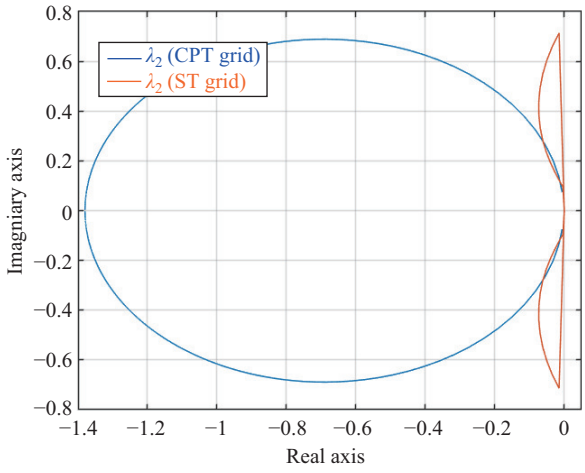

Fig. 7. System characteristic locus (λ_2) of PLL-synchronized converter being connected to different grids (blue – CPT-fed grid, orange – ST-fed grid).

In case of meshed operation, the ST LV converter and the CPT are in parallel and thus $\boldsymbol{Z}_{\text{eq}}$ in (17) should be updated by the parallel impedance of ST and CPT. The system characteristic loci of a meshed grid with PLL-synchronized converter are presented in Fig. 8. It can be seen that none of the them encircles the critical point $(-1,\ j0)$, showing the meshed grid is stable. This indicates the meshed operation can not only optimize the power flow in the distribution grid but also enhance the hosting capability of PLL-synchronized converters.

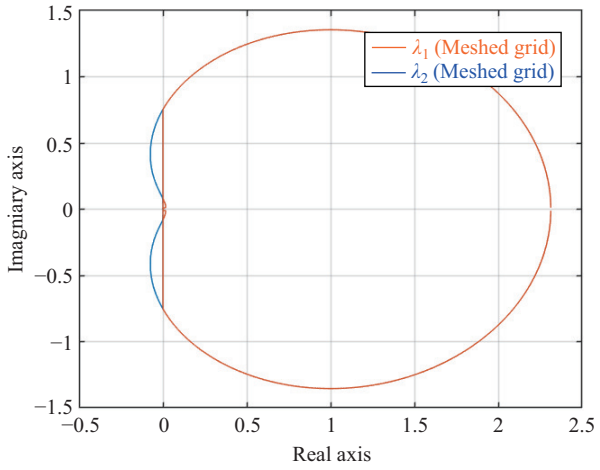

Fig. 8. System characteristic loci of PLL-synchronized converter being connected a meshed grid.

V. Simulation and Experimental Results

In this section, the proposed voltage control, as well as synchronization mechanism, will be verified by simulation and experimental results, in the scenario of overload CPT. Moreover, the stability of PLL-synchronized converter being connected to such a grid under different conditions will be assessed.

A. Simulation Results

First, the CPT overloading case will be studied. In this case study, the passive load being connected to the ST-fed grid is 1.5 kW, while the one being connected to the CPT-fed grid is 6 kW. The security limit of the CPT is 10 A (rms). Initially, the CPT current is 12.4 A (rms) which indicates the CPT is overloaded. The switch between the two feeders will be closed so that the ST can support the CPT-fed grid and alleviate the CPT overloading issue. The timeline of the NOP closure procedure is given in Fig. 9.

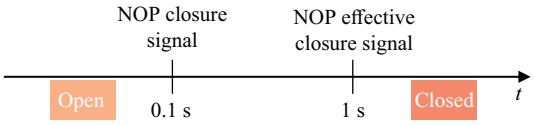

Fig. 9. Timeline of the NOP closure procedure in the case studies.

As seen in Fig. 9, the ST receives the NOP closure signal at 0.1 s, and the ST LV converter starts to regulate the voltage waveforms in terms of amplitude and phase to presynchronize with the CPT side. At 1 s, the NOP effective closure signal is sent and the NOP switch will be closed. The voltage and current of the LV ST-fed grid during the whole NOP closure procedure is given in Fig. 10. From 0.1 s to 1 s, the amplitude and the phase of the ST voltage are smoothly adjusted, and the amplitude of the ST current depends on the loading condition. After 1 s, the switch is closed and the ST LV converter delivers power from the ST side to the CPT-fed grid through the closed switch. Following the power setpoint curve, the ST current increases from 3.11 A to 8.83 A and therefore, more power can be delivered to the CPT side.

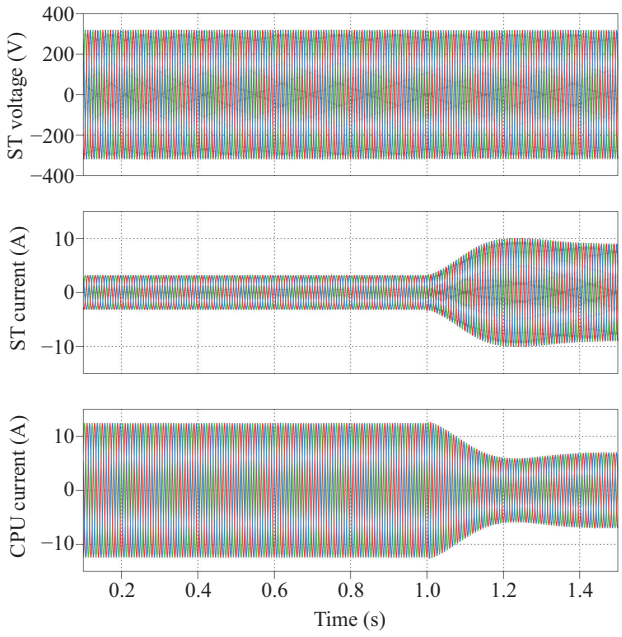

Fig. 10. Simulated waveforms of the LV grid during the whole NOP closure procedure when CPT is overloaded.

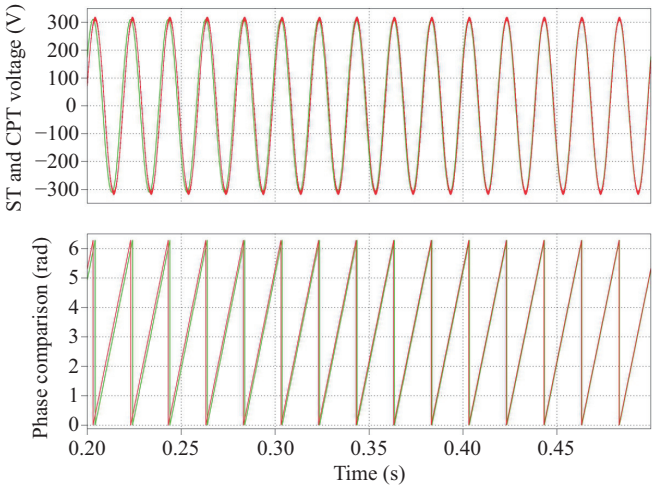

Fig. 11. Voltage waveforms (phase A) of ST- and CPT-fed grids during the presynchronized stage.

The ST and CPT voltage waveforms (phase A), as well as their phase angles in the presynchronized stage, are presented in Fig. 11. The phase of ST voltage can gradually synchronize with that of the CPT side and the two waveforms are completely overlapping at 0.45 s, showing that the voltage waveforms of the two feeders are well synchronized before the NOP effective closure signal.

B. Experimental Results

To verify the effectiveness of the theoretical analysis, experimental validations have been carried out in a laboratory grid fed by ST and CPT, as shown in Fig. 12, using the configuration of Fig. 3. The voltage of the CPT-fed grid is formed by the utility grid through a CPT. Two Danfoss converters are used to emulate the ST LV side converter and the PLL-synchronized converter. The control strategy of Fig. 3 for the ST converter has been implemented in a digital control system using TI digital signal processors. For the sake of convenience, the control of the PLL-synchronized converter has been achieved by the same processor board. Linear loads are connected to the PCC of CPT-fed grid in the beginning, and the security limit of the CPT is 1 A in the scenario.

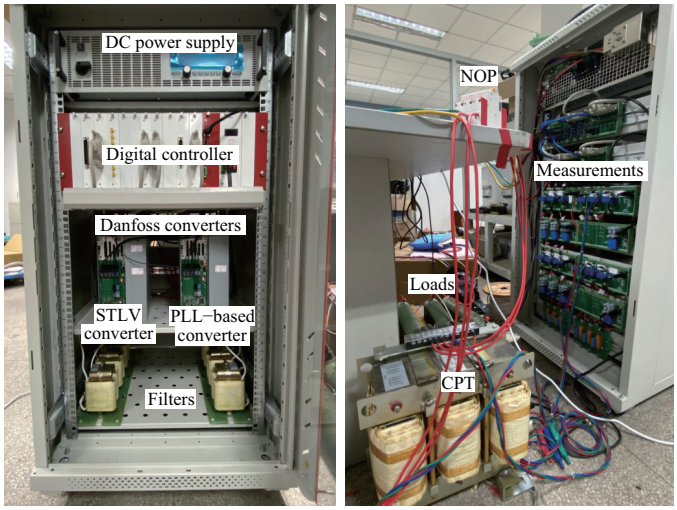

Fig. 12. Experimental setup.

First, the CPT overloading scenario has been tested. Initially, as shown in Fig. 13, the CPT current is 1.2 A (rms) which indicates the CPT is overloaded. At the same time, the ST current is zero since no load is connected to the ST-fed grid. To alleviate CPT overloading, the NOP closure signal

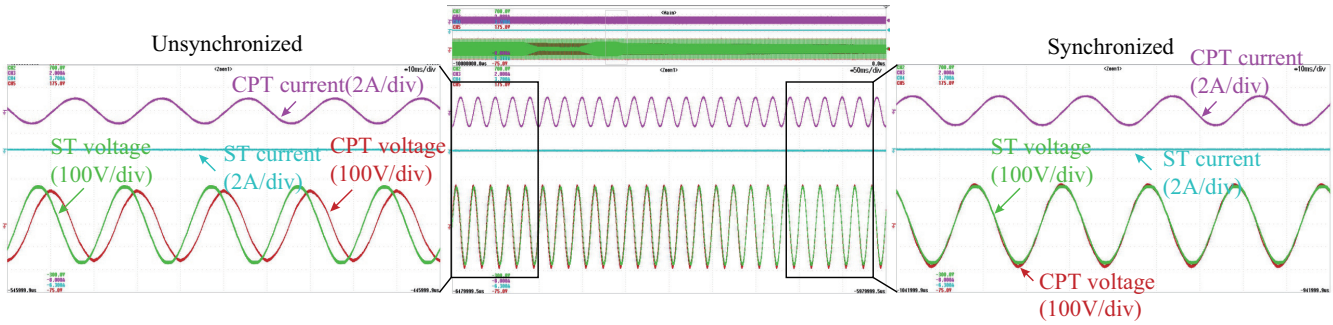

Fig. 13. Experimental waveforms (phase A) of ST- and CPT-fed grids during the presynchronized stage.

will be sent to the ST so that it can start to presynchronize with the CPT voltage and later on support the CPT-fed grid.

As soon as the ST receives the NOP closure signal, the amplitude and the phase angle of the ST voltage are smoothly adjusted as shown in Fig. 13. It can be seen that the two voltage waveforms (ST and CPT voltage) can be well synchronized after a few cycles, where the displacement between the CPT and the ST voltage disappears and the two waveforms are overlapping. Under this circumstance, the NOP can be effectively closed and the waveforms during the transition are given in Fig. 14. It can be seen that the transition from the radial grid to the meshed one is smooth by using the proposed control scheme, where the perturbation is not detected during the whole transition. The voltage waveforms before and after the closure of NOP remain the same, while the CPT current reduces after the closure due to the power sharing of the ST.

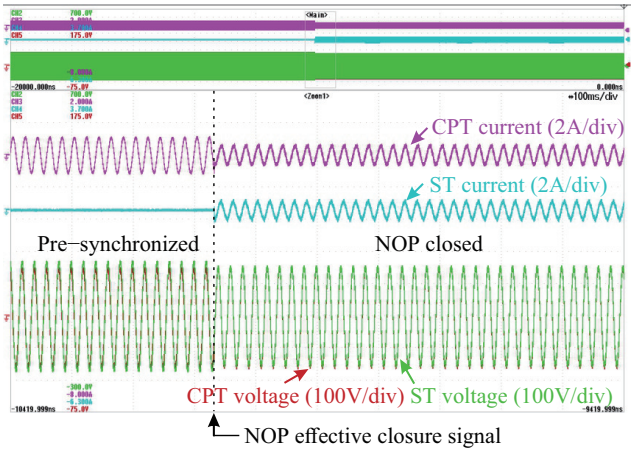

Fig. 14. Experimental waveforms (phase A) of the transition from the radial grid to the meshed operation.

Then, the stability conditions of a PLL-synchronized converter have been evaluated, when it is connected to different grids. The PCC voltage and converter current waveforms are shown in Fig. 15(a) when the PLL-synchronized converter is connected to the CPT-fed grid. In this scenario, the set of control parameters leads to the voltage and current oscillations, indicating the overall system is unstable. However, with the same control parameters, when the converter is connected to the ST-fed grid, the PCC voltage and converter current waveforms are shown in Fig. 15(b). It can be seen the overall system is stable where both the voltage and the current have relatively high power quality.

VI. Conclusion

This paper proposes a voltage control strategy using power-based synchronization for the ST LV converter. The proposed control scheme allows smooth transition between the radial and the meshed operation of a grid fed by both ST and CPT. In this way, the ST in a distribution grid is able to support other feeders and regulate the power flow of the overall network. Moreover, the design criterion of the power setpoints of ST is presented, to guarantee good presynchronization (when it receives NOP closure signal) and good power sharing

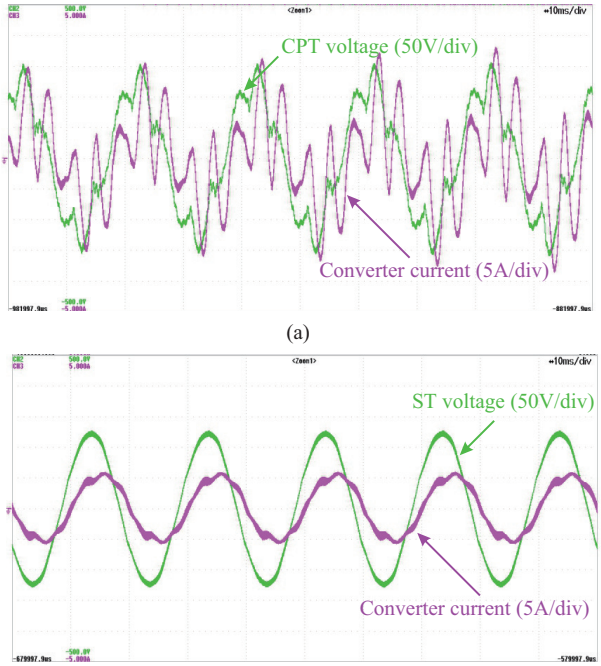

Fig. 15. PCC voltage and converter current (phase A) when the PLL-synchronized converter being connected to different grids: (a) CPT-fed grid and (b) ST-fed grid.

(when NOP is effectively closed). Furthermore, the model and stability of such a system are studied. It shows that the ST-fed grid/feeder can offer a more stable condition to the PLL-synchronized converter, while the CPT-fed grid/feeder cannot. Simulation and experimental results are provided to verify the effectiveness of the proposed control scheme and the stability analysis.

References

[1] M. Liserre, G. Buticchi, M. Andresen, G. De Carne, L. F. Costa, and Z. X. Zou, "The smart transformer: impact on the electric grid and technology challenges," *IEEE Industrial Electronics Magazine*, vol. 10, no. 2, pp. 46–58, Jun. 2016.

[2] Z. X. Zou, G. Buticchi, and M. Liserre, "Control and communication in the smart transformer-fed grid," in *2016 IEEE 21st International Conference on Emerging Technologies and Factory Automation (ETFA)*, 2016, pp. 1–9.

[3] LV ENGINE [Online]. Available: https://www.spenergynetworks.co.uk /pages/lv_engine.aspx.

[4] A. Vukojevic and S. Lukic, "Microgrid protection and control schemes for seamless transition to island and grid synchronization," *IEEE Transactions on Smart Grid*, vol. 11, no. 4, pp. 2845–2855, Jul. 2020.

[5] D. L. Ransom, "Get in step with synchronization," *IEEE Transactions on Industry Applications*, vol. 50, no. 6, pp. 4210–4215, Nov./Dec. 2014.

[6] I. J. Balaguer, Q. Lei, S. T. Yang, U. Supatti, and F. Z. Peng, "Control for grid-connected and intentional islanding operations of distributed power generation," *IEEE Transactions on Industrial Electronics*, vol. 58, no. 1, pp. 147–157, Jan. 2011.

[7] J. Wang, N. C. P. Chang, X. W. Feng, and A. Monti, "Design of a generalized control algorithm for parallel inverters for smooth microgrid transition operation," *IEEE Transactions on Industrial Electronics*, vol. 62, no. 8, pp. 4900–4914, Aug. 2015.

[8] G. G. Talapur, H. M. Suryawanshi, L. Xu, and A. B. Shitole, "A reliable microgrid with seamless transition between grid connected and islanded mode for residential community with enhanced power quality," *IEEE*

Transactions on Industry Applications, vol. 54, no. 5, pp. 5246–5255, Sep./Oct. 2018.

[9] M. Ganjian-Aboukheili, M. Shahabi, Q. Shafiee, and J. M. Guerrero, "Seamless transition of microgrids operation from grid-connected to islanded mode," *IEEE Transactions on Smart Grid*, vol. 11, no. 3, pp. 2106–2114, May 2020.

[10] G. De Carne, X. Gao, Z. X. Zou, M. Liserre, A. Kazerooni, and M. Eves, "Smart transformer requirements for integration in distribution grids and power quality improvement," in *2019 IEEE Milan PowerTech*, 2019, pp. 1–6.

[11] S. Giacomuzzi, G. De Carne, S. Pugliese, G. Buja, M. Liserre, and A. Kazerooni, "Synchronization of low voltage grids fed by smart and conventional transformers," *IEEE Transactions on Smart Grid*, vol. 12, no. 4, pp. 2941–2951, Jul. 2021.

[12] J. M. Guerrero, J. C. Vasquez, J. Matas, L. G. De Vicuna, and M. Castilla, "Hierarchical control of droop-controlled AC and DC microgrids-a general approach toward standardization," *IEEE Transactions on Industrial Electronics*, vol. 58, no. 1, pp. 158–172, Jan. 2011.

[13] T. L. Vandoorn, J. D. M. De Kooning, B. Meersman, J. M. Guerrero, and L. Vandevelde, "Voltage-based control of a smart transformer in a microgrid," *IEEE Transactions on Industrial Electronics*, vol. 60, no. 4, pp. 1291–1305, Apr. 2013.

[14] S. Dong, J. Y. Jiang, and Y. C. Chen, "Analysis of synchronverter self-synchronization dynamics to facilitate parameter tuning," *IEEE Transactions on Energy Conversion*, vol. 35, no. 1, pp. 11–23, Mar. 2020.

[15] Q. C. Zhong and G. Weiss, "Synchronverters: inverters that mimic synchronous generators," *IEEE Transactions on Industrial Electronics*, vol. 58, no. 4, pp. 1259–1267, Apr. 2011.

[16] F. Blaabjerg, R. Teodorescu, M. Liserre, and A. V. Timbus, "Overview of control and grid synchronization for distributed power generation systems," *IEEE Transactions on Industrial Electronics*, vol. 53, no. 5, pp. 1398–1409, Oct. 2006.

[17] L. Harnefors, M. Bongiorno, and S. Lundberg, "Input-admittance calculation and shaping for controlled voltage-source converters," *IEEE Transactions on Industrial Electronics*, vol. 54, no. 6, pp. 3323–3334, Dec. 2007.

[18] Z. X. Zou and M. Liserre, "Modeling phase-locked loop-based synchronization in grid-interfaced converters," *IEEE Transactions on Energy Conversion*, vol. 35, no. 1, pp. 394–404, Mar. 2020.

[19] R. Rosso, M. Andresen, S. Engelken, and M. Liserre, "Analysis of the interaction among power converters through their synchronization mechanism," *IEEE Transactions on Power Electronics*, vol. 34, no. 12, pp. 12321–12332, Dec. 2019.

[20] R. Rosso, S. Engelken, and M. Liserre, "Robust stability investigation of the interactions among grid-forming and grid-following converters," *IEEE Journal of Emerging and Selected Topics in Power Electronics*, vol. 8, no. 2, pp. 991–1003, Jun. 2020.

Zhixiang Zou received B.Eng. and Ph.D. degrees in Electrical and Engineering from Southeast University, Nanjing, China, in 2007 and 2014, respectively, and the Dr.-Ing. degree (summa cum laude) from Kiel University, Germany, in 2019. He was an Engineer in the State Grid Electric Power Research Institute, Nanjing, China, from 2007 to 2009. He was a Research Fellow at the Chair of Power Electronics, Kiel University, Germany, from 2014 to 2019. He is now an Associate Professor in the School of Electrical Engineering at Southeast University. His research interests include smart transformers, microgrid stability, modeling and control of power converters. Dr. Zou is a Member and Industrial Liaison of the IEEE-IES Technical Committee on Renewable Energy Systems, and a Secretary of IEEE Standard P3105. He was awarded with Gold Medal in Geneva International Exhibition of Inventions and IEEE PES Outstanding Academic Publishing Award. He serves as Associate Editor for *IEEE Transactions on Industrial Electronics, IEEE Open Journal of Power Electronics*, and *IEEE Access*.

Xingqi Liu received the B.S. degree in Electrical Engineering from Shijiazhuang Tiedao University, Shijiazhuang, China, in 2021 and the M.S. degree in Electrical Engineering from Southeast University, Nanjing, China, in 2023. She is currently working toward the Ph.D. degree in Power Electronics with the University of Nottingham Ningbo China. Her research interests include smart transformers, DC-DC converter and the stability of power converters.

Jian Tang received the B.S. and M.S. degrees in Electrical Engineering from Southeast University, Nanjing, China, in 2021 and 2024, respectively. Since 2024, he has been with State Grid Changzhou Power Supply Company. His research interests include the stability of power converters and the application of artificial intelligence on power converters.

Giovanni De Carne received B.Sc. and M.Sc. degrees in Electrical Engineering from the Polytechnic University of Bari, Italy, in 2011 and 2013, respectively, and the Ph.D. degree in Electrical Engineering and Information Technology from the Chair of Power Electronics, Kiel University, Germany, in 2018. He is currently W3 (full) Professor with the Institute for Technical Physics, Karlsruhe Institute of Technology, Karlsruhe, Germany, where he leads the "Real Time Systems for Energy Technologies" Group and the "Power Hardware In the Loop Lab". He is currently supervising Ph.D. students, managing academic and industrial projects, and developing multi-MW power hardware in the loop testing infrastructures for energy storage systems and hydrogen-based drives. He has authored or coauthored more than 100 peer-reviewed scientific papers. His research interests include power electronics integration in power systems, solid-state transformers, real-time modeling, and power hardware in the loop. He has been the Technical Program Committee Chair for several IEEE conferences, and Associate Editor for *IEEE Open Journal of Power Electronics* and several other IEEE and IET journals.

Marco Liserre obtained the M.Sc. and Ph.D. degrees in Electrical Engineering from the Politecnico di Bari in 1998 and 2002, respectively. He has been Associate Professor at the Politecnico di Bari and, since 2012, Professor of Reliable Power Electronics at Aalborg University (Denmark). Since 2013 he is Full Professor and holds the Chair of Power Electronics at the University of Kiel (Germany). He has been offered and declined professorships at several universities. He has published more than 700 technical papers (1/3 of them in international refereed journals), one book and 7 granted patents (4 with companies). These works have received more than 50,000 citations. He was selected as a Highly Cited Researcher in the field of Engineering (Clarivate Web of Science) from 2014 to 2021. In 2023, he joined the Fraunhofer ISIT on a part-time basis as deputy director and director of the new division "Electronic Energy Systems", as well as of the Kiel branch of the Fraunhofer ISIT. He is a Member of IAS, PELS, PES and IES. He has received 16 awards from IEEE, PCIM and EPE-PEMC, including the prestigious 2018 IEEE-IES Mittelmann Achievement Award and the 2023 IEEE-PELS R. David Middlebrook Achievement Award. In 2023, he was awarded the title of "Ufficiale" by the President of the Italian Republic. In 2025 he will be Chairman of Powertech 2025 in Kiel.

Zheng Wang received B.Eng. and M.Eng. degrees from Southeast University, Nanjing, China, in 2000 and 2003, respectively, and the Ph.D. degree from the University of Hong Kong, Hong Kong, China, in 2008, all in Electrical Engineering. From 2008 to 2009, he was a Postdoctoral Fellow in Ryerson University, Toronto, ON, Canada. He is currently a full Professor in the School of Electrical Engineering, Southeast University, China. His research interests include electric drives, power electronics, and distributed generation. In these fields, he has authored over 120 internationally refereed papers, one English book by IEEE-Wiley Press, and two English book chapters. Professor Wang received IEEE PES Chapter Outstanding Engineer Award, First-class Science and Technology Award of Jiangsu Province in China, and Outstanding Young Scholar Award of Jiangsu Natural Science Foundation of China. He is an IET Fellow and an Associate Editor of *IEEE Transactions on Industrial Electronics*.

Ming Cheng received B.Sc. and M.Sc. degrees from the Department of Electrical Engineering, Southeast University, Nanjing, China, in 1982 and 1987, respectively, and the Ph.D. degree from the Department of Electrical and Electronic Engineering, University of Hong Kong, Hong Kong, China, in 2001, all in Electrical Engineering. Since 1987, he has been with Southeast University, where he is currently a Chief Professor at the School of Electrical Engineering and the Director of the Research Center for Wind Power Generation. From January to April 2011, he was a Visiting Professor with the Wisconsin Electric Machine and Power Electronics Consortium, University of Wisconsin, Madison, WI, USA. His teaching and research interests include electrical machines, motor drives for EV, renewable energy generation, and servo motor and control. He has authored or co-authored more than 500 technical papers and 7 books, and is the holder of 150 patents in these areas. Professor Cheng is a Fellow of the Institution of Engineering and Technology. He has served as the Chair and an Organizing Committee Member for many international conferences. He was a Distinguished Lecturer of the IEEE Industry Application Society in 2015/2016.